L. Devaraj, Q. M. Khan, A. R. Ruddle, A. Duffy, R. Perdriau, and M. Koohestani, "Application of probabilistic models for multi-tone electromagnetic immunity analysis," IEEE Trans. Electromagn. Compat., 2022. doi: 110.1109/TEMC.2022.3211458.

Application of Probabilistic Models for Multitone Electromagnetic Immunity Analysis

Lokesh Devaraj, *Student Member, IEEE*, Qazi Mashaal Khan, *Graduate Student Member, IEEE*, Alastair R. Ruddle, *Senior Member, IEEE*, Alistair P. Duffy, *Fellow, IEEE*, Richard Perdriau, *Senior Member, IEEE*, and Mohsen Koohestani, *Senior Member, IEEE*

***Abstract*—The operational environment of modern electronic systems may include multiple frequency electromagnetic disturbances. However, immunity measurements usually employ single frequency continuous waveforms (i.e. *single-tones*). The performance of two oscillator circuits with different topologies (one simulated and one measured) were used as case studies to investigate immunity to simultaneous single-tone disturbances (i.e. *multitones*) using probabilistic Bayesian network models. For the multitone analysis, the noisy-OR model was first used to identify the type of causal interactions between simultaneously occurring single-tones. Probabilistic theories derived from the recursive noisy-OR model, which inherits the independence assumptions of the noisy-OR and any known causal dependence between simultaneously occurring single-tones, were then used to predict the probability of higher order multitone failures. For the two case studies, the probability of three-tone failures was estimated using the single-tone and two-tone failure probability values. An improved adaptive recursive noisy-OR model was also proposed to overcome the practical difficulties of obtaining multitone failure probabilities, from either simulations or measurements.**

***Index Terms*—Bayesian networks (BN), electromagnetic interference (EMI), failure probability, multitone immunity, noisy-OR, recursive-noisy-OR (RNOR), synergistic effect.**

I. Introduction

THE electromagnetic (EM) immunity of integrated circuits (ICs) plays an important role in maintaining the functional performance of electronic systems in harsh EM environments. For a given failure criterion, the probability of IC failures can vary depending on the frequencies of the coupled EM disturbances, as well as other external factors such temperature and humidity. Currently, IC immunity to radiated and conducted EMI is assessed using single frequency continuous waveforms [1] (i.e. *single-tones*) . In practice, however, the EM environment may include multiple disturbances that could occur simultaneously.

The significance of investigating the effect of two or more simultaneously occurring single-tone disturbances, i.e. *multitone* EMI disturbances [2], [3] and its benefits [4] are well known. For multitone disturbances, potential for intermodulation effects should also be considered [5], [6]. The international standard IEC 61000-4-3:2020 [7] now includes verification with multitone disturbances, although the main purpose here is to reduce the overall test time. Nevertheless, for a risk-based approach [8], multitone testing may potentially be more representative of real-world EM environments.

The main challenge of multitone immunity analysis is the potentially infinite number of single-tone combinations that can be considered. For multitone measurements, however, the number of simultaneous tones that can be used is limited due to amplifier saturation. Consequently, simulation offers a more practicable approach to investigate relatively large sets of tone combinations, as well as higher orders of multitone disturbances.

In the past, statistical models have been used to analyse the immunity of integrated circuits with respect to single-tone EMI [9], [10]. More recently, probabilistic graphical models, such as Bayesian networks (BN), have been used in applications such as the analysis of intentional EMI threats [11], [12]. This paper discusses the application of well-established probabilistic models and theories for two main purposes. Firstly, to identify the type of causal dependence between simultaneously occurring single-tone disturbances and its impact on the component's probability of failure due to EMI. This is achieved using the well-known noisy-OR model [13], which assumes causal independence to calculate the probability of multitone EMI failure. Secondly, to overcome some of the practical difficulties of obtaining multitone EMI failure data, use of the recursive-noisy-OR (RNOR) [14], and its descendants, the adaptive-RNOR (ARNOR) [15] and the extended-RNOR [16] are considered. In common, these theories inherit the independence assumptions of the noisy-OR model and can include any available causal dependence information to calculate higher-order multitone failure probability. This paper provides the theoretical framework for a BN-based analysis of multitone immunity, which is illustrated and validated using

The research leading to these results has received funding from the European Union's Horizon 2020 research and innovation programme under the Marie Skłodowska-Curie grant agreement No 812790 (MSCA-ETN PETER). (*Corresponding author: Lokesh Devaraj.*)

Lokesh Devaraj is with HORIBA MIRA Limited, Nuneaton, CV10 0TU, UK, and also with De Montfort University, The Gateway, Leicester, LE1 9BH, UK (email: lokesh.devaraj@horiba-mira.com).

Qazi Mashaal Khan is with the ESEO School of Engineering, Department of Electrical and Electronic Engineering, RF-EMC Research group, 49107 Angers, France, and also with the Institut National des Sciences Appliquées, Department of Electronics Engineering, 35708 Rennes, France (email: qazi-mashaal.khan@eseo.fr).

Alastair Ruddle is with HORIBA MIRA Limited, Nuneaton, CV10 0TU, UK (e-mail: alastair.ruddle@horiba-mira.com).

Alistair Duffy is with De Montfort University, The Gateway, Leicester, LE1 9BH, UK (e-mail: apd@dmu.ac.uk).

Richard Perdriau and Mohsen Koohestani are with the ESEO School of Engineering, Department of Electrical and Electronic Engineering, 49107 Angers, France, and also with the Institute of Electronics and Telecommunications of Rennes, University of Rennes 1, 35042 Rennes, France (email: richard.perdriau@eseo.fr; mohsen.koohestani@eseo.fr).

Digital Object Identifier 10.1109/TEMC.2022.XXXXXXX

L. Devaraj, Q. M. Khan, A. R. Ruddle, A. Duffy, R. Perdriau, and M. Koohestani, "Application of probabilistic models for multi-tone electromagnetic immunity analysis," IEEE Trans. Electromagn. Compat., 2022. doi: 110.1109/TEMC.2022.3211458.

numerical simulation results for a current starved voltage controlled oscillator (CSVCO) circuit subjected to up to three simultaneous EM disturbances at different frequencies. In addition, application of the probabilistic models to analyse the measured multitone immunity performance of a different circuit, a ring oscillator (RO), is also outlined. A more extensive investigation of measured multitone immunity using these techniques is provided in [17], which also takes account of thermal impacts on multitone immunity.

The paper is organized as follows. The functional description of the CSVCO used for the first case study, including its failure criterion and the simulation of EMI noise samples considered for the multitone immunity analysis, are discussed in Section II. The probabilistic models are discussed in Section III and illustrated with suitable examples from the simulation results of the CSVCO circuit in Section IV. In Section V, a new probabilistic model is proposed, the improved-ARNOR (I-ARNOR), which is found (using simulations results) to increase the mean prediction accuracy of estimates for the probability of higher-order multitone EMI failures when compared to the existing methods. The improved prediction accuracy of the I-ARNOR model is also confirmed in Section VI, using experimental data collected for the second case study based on the multitone immunity performance of a different (RO) circuit. Finally, Section VII summarises the conclusions.

II. Case Study A - Simulated Data

A current-starved voltage controlled oscillator (CSVCO) [18] circuit was chosen as a case study for the multitone immunity analysis. It is important to note that several practical factors limit the reliability of measurements of multi-tone immunity performance for such devices, including trade-off between the oscilloscope resolution and acquisition time of the output signal, cable losses, temperature variations, and the limited bandwidth of the currently available arbitrary waveform generators. In particular, for experimental monitoring of VCO circuits with high output frequencies with minimum parasitic filtering effects (i.e., due to the output pad capacitance), a frequency divider (FD) has to be used (as shown in Fig. 1).

For multitone disturbances, the inter-modulation products (with much higher frequencies than the expected output frequency of the oscillator) not only play a very vital role in determining the circuit performance but are also prone to the filtering effects of the FD. An earlier study [19], the simulated multitone immunity analysis of two different integrated oscillator designs (including the CSVCO used in the current study), using data collected both before and after the FD circuit, indicate that the FD is expected to have a significant impact on practical measurements. In real-world applications, however, the FD is not used.

As simulations allow most of these factors to be either excluded or accounted for, computational models were used for this study instead of experimental measurements to gain greater insight and reliability for the validation of probabilistic models for multitone immunity analysis and performance prediction.

A. Model Description

A VCO is generally used to drive internal blocks such as phase locked loops. The PETER_ESEO IC is designed to be manufactured in silicon-on-insulator CMOS 5 V using 180 nm technology kit, provided by the XFAB foundry [20]. The function of the CSVCO is to provide an output voltage at a nominal frequency of F_1 = 703 MHz, for a given control input V_C = 1.8 V and isolated supply voltage V_{DDI} = 5 V.

The IC, consisting of various independent analog circuits, is surrounded by a padring which includes electrostatic discharge protection structures to both the supply and ground rails (Fig. 1). The global power supply (V_{DD} = 5 V) is connected to the feeding ports V_O, V_R, & V_5 to power up the padring and the digital blocks with reduced noise coupling. Hence, to isolate the global feeding ports from injected EM disturbance, an isolated biasing supply V_{DDI} that powers up the CSVCO circuit was used.

The circuit was designed using Cadence Virtuoso, a commercial software tool that is widely used in the industry to design ICs, and the immunity simulations were carried out using Spectre [21]. The package chosen for this research chip is a ceramic quad flat package. It was modelled using the IC-EMC software [22], which helps in representing a realistic package model through lumped parasitic elements.

The EMI simulations, using the setup shown in Fig. 1, allowed for up to three sinusoidal waveforms to be injected into V_{DDI}, which provides biasing to the CSVCO only. A virtual voltage probe was placed before the FD to accurately monitor the voltage fluctuations without the filtering affects caused by the FD, output pad and package. For single-tone simulations the amplitudes of tones 2 and 3 were set to 0 V, and for two-tone cases the amplitude of tone 3 was set to 0 V. The pins V_C and V_{DD}, were assumed to be isolated from EMI. Each simulation represented a period of 1 μs, and the EMI noise was added to the input supply after the initial transient response time of the IC (300 ns). This was the minimum time required for the output voltage of the CSVCO to stabilize. The fast Fourier transform at discrete-time steps (1.4 –1.5 ns) was applied using the Cadence *SKILL* mode function to obtain the output frequency under EMI conditions, F_E, for each respective time-step over the 700 ns steady-state period. Hence, 466 to 500 time-steps were collected for each EMI simulation, which took around 6 minutes, including set-up, on a high-performance workstation.

The frequencies for the multitone simulations were selected from the range 50-950 MHz as this CSVCO design was found to be susceptible in this band in an earlier study [20] and is within the frequency scope of [1].

B. EMI Failure Criterion

The immunity of the circuit was determined by comparing F_E, with respect to F_i. For the CSVCO, $F_i = F_1$. The relative deviation of F_E from the desired F_i, is then calculated as a percentage using:

$$\Delta F = 100 \left| \frac{F_E - F_i}{F_i} \right| \quad (1)$$

L. Devaraj, Q. M. Khan, A. R. Ruddle, A. Duffy, R. Perdriau, and M. Koohestani, “Application of probabilistic models for multi-tone electromagnetic immunity analysis,” IEEE Trans. Electromagn. Compat., 2022. doi: 110.1109/TEMC.2022.3211458.

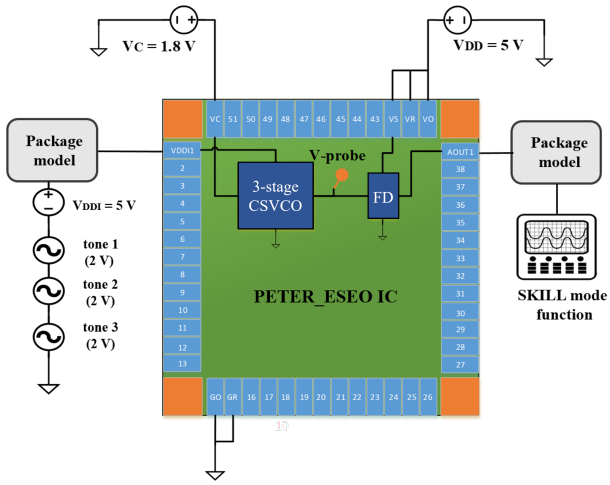

Fig. 1. Multitone EMI simulation setup for the CSVCO circuit.

The CSVCO is considered to have failed every time ΔF exceeds the acceptable tolerance of $\pm 5\%$. The probability of failure due to EMI is then estimated by dividing the number of such failures by the total number of time-steps under EMI.

C. Single-Tone EMI Simulations

An initial set of single-tone EMI simulations were carried out at frequency values that were uniformly distributed in the range of 10 MHz to 1 GHz with a step size of 10 MHz. The peak-to-peak amplitude was 2 V, to avoid exceeding the immunity requirement of [1] with up to three tones, and the initial phase was zero. For single-tone EMI, the impact of the initial phase is negligible if the monitored time period encompasses multiple EMI cycles.

Sample results (for arbitrarily selected frequencies) are illustrated in Fig. 2, for 450 MHz, and in Fig. 3, for 800 MHz. The dashed red lines in these plots indicate the tolerance limits, i.e. ($\pm 5\%$ of F_0). Using the failure criterion, the probabilities of EMI failure at 450 MHz and 800 MHz were determined to be 65.33%, and 54.02%, respectively. Due to the non-linear behaviour of the VCO circuit, F_E varies over the duration of the steady-state EMI response. This effect can be seen in Figs. 2–3, which exhibit minor variations in the VCO output frequency between successive cycles of the EMI.

Using the failure criterion (1), the probability of EMI failure estimated for each of the single-tone simulations is shown in Fig. 4. The results may vary if different amplitudes are considered, but for this paper the amplitude is considered constant.

D. Multitone EMI Simulations

For multitone analysis, the total number of non-repeating combinations $N(n,r)$ for n frequencies and multitone disturbances up to order r can be calculated using:

$$N(n,r) = \frac{n!}{r!(n-r)!} \tag{2}$$

where, $m!$ denotes the factorial of an integer m. Hence it can be seen that the number of combinations can rapidly become unmanageable as n and r increase.

For the purposes of a practical illustration, limiting the

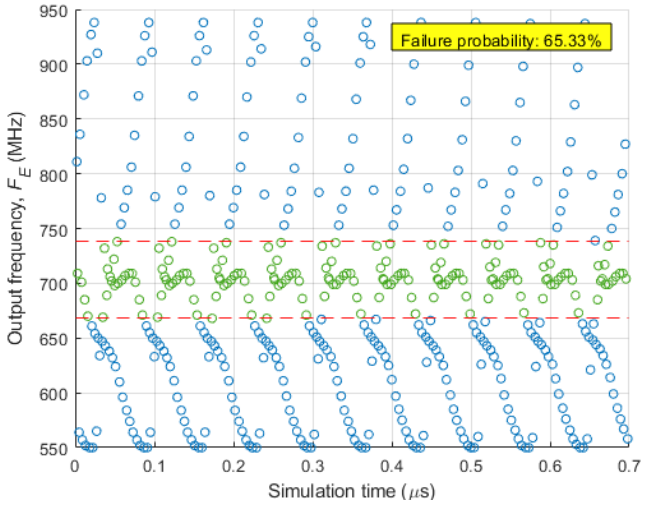

Fig. 2. VCO output for single-tone disturbance at 450 MHz.

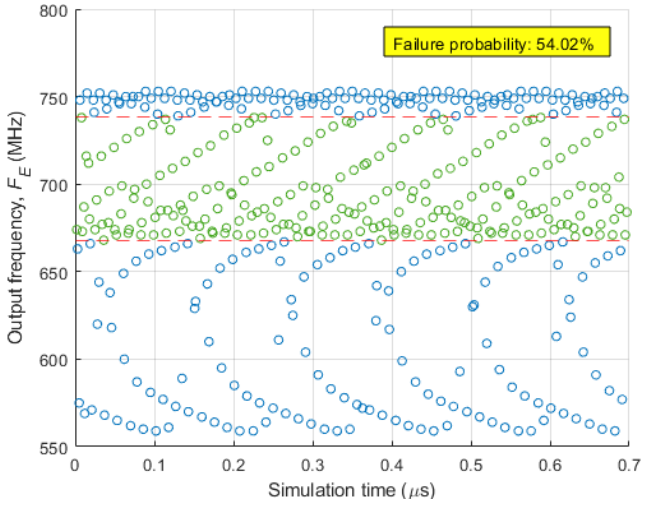

Fig. 3. VCO output for single-tone disturbance at 800 MHz.

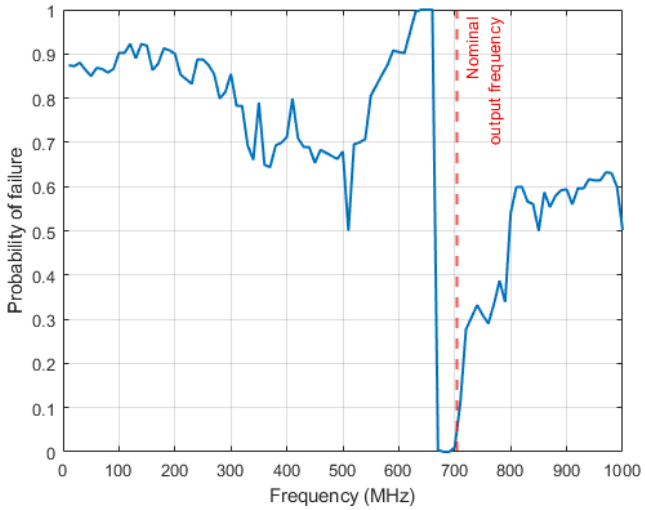

Fig. 4. Probability of VCO failure due to single-tone EMI

L. Devaraj, Q. M. Khan, A. R. Ruddle, A. Duffy, R. Perdriau, and M. Koohestani, "Application of probabilistic models for multi-tone electromagnetic immunity analysis," IEEE Trans. Electromagn. Compat., 2022. doi: 110.1109/TEMC.2022.3211458.

number of frequencies to $n = 15$ and the multitone order to $r = 3$ results in a requirement for a total of 575 simulations, comprised of 15 single-tones, as well as 105 two-tone and 455 three-tone frequency combinations.

A generalized expression (i.e. including single-tone) for the waveform of a multitone disturbance of order $r \in \{1, 2, 3\}$ is:

$$V(t, r) = A \sum_{k=1}^{r} sin(2\pi f_k t + \phi_k) \quad (3)$$

where A represents the 2 V amplitude of each of the tones and the initial phase, ϕ_k, was $\phi_1 = 0$ for single-tones (i.e. $k = 1$) and to reduce the number of simulations for this study, a random initial phase value was assigned from the range $0 < \phi_k < 360°$ for each superimposed tone (i.e. $k>1$). Nonetheless, the initial phase difference between simultaneous tones can have an impact on the multitone EMI failure probability values. The results shown in Fig. 5, for three sample two-tone disturbances ($\{450, 800\}$, $\{50, 600\}$ and $\{750, 900\}$) illustrate the failure probability for various initial phase difference between the pairs of tones (indicated using circles) as well as the mean values (dashed lines).

An example of the output frequency F_E over time is illustrated in Fig. 6 for the two-tone $\{450, 800\}$, which contains the single-tones of Figs. 2–3. In order to understand the interactions that produce the multitone results it is necessary to introduce probabilistic models.

III. Probabilistic Models

A. Limitations of Multi-Causal Analysis

In many real-world applications, the causal relationships between multiple causes and a common effect are visualized using probabilistic graphical models called the Bayesian networks (BN) [23]. The BN shown in Fig. 7 consists of n causes $\{C_1, C_2, ..., C_n\}$, each of which can individually lead to a common effect E. The nodes in Fig. 7 are binary variables, such that $C_n = \{c_n, \bar{c_n}\}$ denotes the presence (c_n) and the absence ($\bar{c_n}$) of a cause n. Similarly, $E = \{e, \bar{e}\}$ denotes the effect being observed and unobserved, respectively.

For a complete BN [23], the conditional probability distribution (CPD) table corresponding to graphical node E need to be filled with 2^n entries. Each of these entries correspond to the probability of observing the effect given a subset of causes that are present. Any inference for the multi-causal analysis can be made only if all the probability values are provided.

For example, the case $n = 2$ requires four probability entries for node E: $\mathcal{P}(e|c_1, c_2)$, $\mathcal{P}(e|\, c_1, \bar{c_2})$, $\mathcal{P}(e|\bar{c_1}, c_2)$ and $\mathcal{P}(e|\, \bar{c_1}, \bar{c_2})$. Since the number of CPD entries for observing the effect increases exponentially with the number of causes, it becomes impractical to provide the probability entries corresponding to every possible combination of causes.

As a shorthand in this paper, the CPD for node E is expressed by including only the causes that are present, i.e., $\mathcal{P}(e|\, c_1, \bar{c_2})$ is simply written as $\mathcal{P}(e|\, c_1)$.

B. Application to Multitone Immunity

Similar problems may arise during multitone immunity analyses if we consider each frequency resulting in a single-tone disturbance as an individual cause, and the component failure due to EMI as the effect. For instance, the total number of CPD entries required for 15 frequencies is 2^{15} = 32,768, and this increases to 1,048,576 entries for an additional 5 frequencies. In addition, varying the relative amplitude, polarization, initial phase etc. of each tone will further increase the number of possible multitone combinations exponentially.

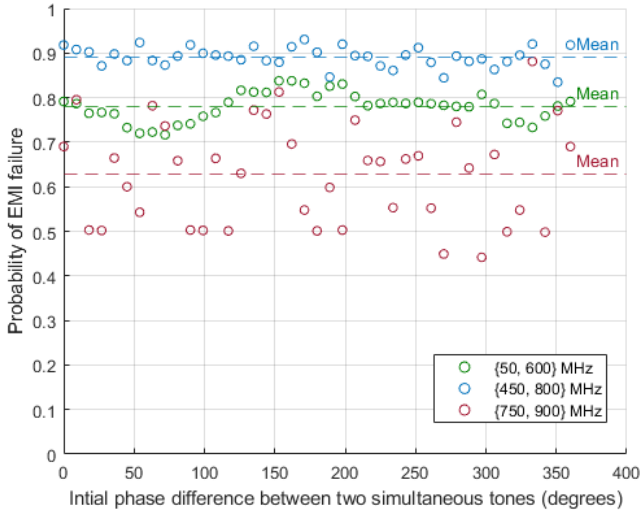

Fig. 5. Impact of initial phase difference between multitones on probability of EMI failure.

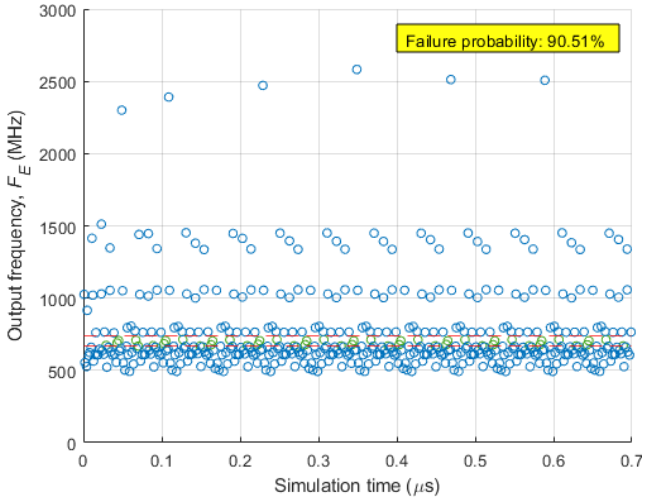

Fig. 6. VCO output for two-tone disturbance at frequencies $\{450, 800\}$ MHz.

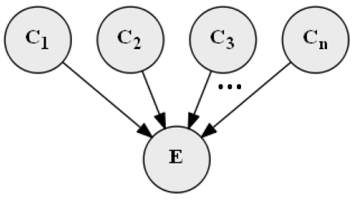

Fig. 7. Graphical model to map the causal relationship between multiple causes and a common effect.

L. Devaraj, Q. M. Khan, A. R. Ruddle, A. Duffy, R. Perdriau, and M. Koohestani, "Application of probabilistic models for multi-tone electromagnetic immunity analysis," IEEE Trans. Electromagn. Compat., 2022. doi: 110.1109/TEMC.2022.3211458.

Consequently, making a comprehensive multitone analysis using measurements is impracticable, but simulation can potentially provide a more convenient alternative. However, simulation also becomes computationally intensive, time consuming, and ultimately impracticable for large numbers of frequencies. Nonetheless, there are potential solutions that have been proposed to overcome the limitations of such multi-causal BN analysis, which are discussed further below.

C. Noisy-OR Model

The so-called *noisy-OR* model [13] was introduced to overcome the limitations of exponential probability assessments in causal BNs. According to this model, if the causal mechanisms of simultaneously occurring causes (e.g., multitones) are independent of each other, then the probability $\mathcal{N}(e|\,\mathbf{x})$ of observing the effect E (e.g., EMI failure) given any subset $\mathbf{x}$ of up to r simultaneously occurring causes is:

$$\mathcal{N}(e|\,\mathbf{x}) = 1 - \{(1-\lambda)\prod_{k=1}^{r}[1-\mathcal{P}(e|\,c_k)]\} \tag{4}$$

where $\mathcal{P}(e|\,c_k)$ represents the probability at which cause c_k (for $k \in \{1, 2..r\}$) in $\mathbf{x}$ can individually lead to the effect, and λ is the *leak probability* [24] of observing the effect in the absence of all identified causes. It should be noted that, using (3), only r probability entries, $\mathcal{P}(e|\,c_1)$ to $\mathcal{P}(e|\,c_r)$, are required to complete all the CPD entries for node E.

For multitone immunity analysis, if the failure probability due to n single-tones are known, then the probability of EMI failure for any r-tone combination can be determined using (4). However, causal independence is questionable for the estimation of multitone failure probability, and causal dependence between multitones can have both positive and negative impacts on the probability of multitone EMI failure.

D. Probabilistic Causality

To identify the nature of causal dependence between multiple causes, the available probability values can be compared with those calculated from the noisy-OR independence assumptions [14], [25]. Based on the comparison, causal interactions can be classified either as *positive causality* or *inhibition*.

1) Positive Causality: The causal interaction between multiple causes is said to have a positive causality [14], if the probability of observing the effect (or failure) is higher than the probability of each cause leading to the effect individually. For example, two simultaneously occurring causes $\{C_1, C_2\}$ are said to have positive causality, if $\mathcal{P}(e|\,c_1, c_2) > \mathcal{P}(e|\,c_1), \mathcal{P}(e|\,c_2)$. Note that, the probability values estimated using the noisy-OR model, i.e., $\mathcal{N}(e|\,\mathbf{x})$ always satisfy the positive causality condition if $0 < \mathcal{P}(e|\,c_k) < 1$.

Causal interactions having positive causality can be further sub-classified [14]–[16] as *synergy* when $\mathcal{P}(e|\,\mathbf{x}) > \mathcal{N}(e|\,\mathbf{x})$, and *interference* otherwise. To avoid possible confusion with EMI, the term *asynergy* is adopted in this paper instead of the more widely used term *interference*.

2) Inhibition: In contrast to positive causality, multiple causes may also counteract each others effects. The probability of observing the effect is then smaller than the probabilities of the individual causes leading to the effect.

E. Recursive Noisy-OR Model and Related Models

The *recursive noisy-OR* (RNOR) [14] was introduced to achieve more accurate construction of the CPD tables. To calculate the CPD entries, the RNOR rule inherits the causal independence assumptions of the noisy-OR model and any known causal dependence information between multiple causes that is available. The RNOR rule is given as:

$$\mathcal{R}(e|\,\mathbf{x}) = \begin{cases} \mathcal{P}(e|\,\mathbf{x}), \\ \text{if available} \\ 1 - \prod_{k=0}^{r-1}\left[\dfrac{1-\mathcal{R}(e|\,\mathbf{x}\setminus\{c_{k+1}\})}{1-\mathcal{R}(e|\,\mathbf{x}\setminus\{c_{k+1}, c_{\text{mod }(k+1,r)+1}\})}\right], \\ \text{otherwise} \end{cases} \tag{5}$$

where, the symbol $\setminus$ denotes set subtraction and $\text{mod}(m, n)$ denotes the modulo operation on integers m and n. Use of the modulo function requires an index running from 0 in the product, but the resulting indices are incremented by 1 to maintain consistency with the cause numbering $\{C1, C2, C3\}$. The RNOR rule simply reduces to the noisy-OR if no additional information is provided.

There are two main drawbacks of RNOR rule. Firstly, it is only applicable when positive causality is true. This is because, in the case of inhibition, the probability values may lie outside the range [0,1], thus violating the axioms of probability theory. To avoid this, a method called the *adaptive-RNOR* (ARNOR) rule has been introduced [15]. According to this scheme, any probability $\mathcal{P}(e|\,\mathbf{x})$ identified as inhibition is simply replaced with the noisy-OR $\mathcal{N}(e|\,\mathbf{x})$ value. The ARNOR rule is:

$$\mathcal{R}_A(e|\,\mathbf{x}) = \begin{cases} \mathcal{P}(e|\,\mathbf{x}), \\ \text{if available and } \mathbf{x}\text{: positive causality} \\ \mathcal{N}(e|\,\mathbf{x}), \\ \text{if } \mathcal{P}(e|\,\mathbf{x}) \text{ is available and } \mathbf{x}\text{: inhibition} \\ \mathcal{R}(e|\,\mathbf{x}) \\ \text{otherwise} \end{cases} \tag{6}$$

The second drawback of RNOR is that (5) loses its symmetry when the number of causes exceeds 3 (see [16], [26], [27] for more details). Although not an issue in this work, the *extended-RNOR* rule [16] can provide a solution to this.

IV. Multitone Immunity Analysis

In order to limit the number of multitone disturbancess, 15 frequencies were selected spanning the band 50-950 MHz, as detailed in Table I, which also includes their corresponding failure probabilities $\mathcal{P}(e|\mathbf{x})$ for single-tone EMI. Samples of the higher order multitone combinations and their associated failure probabilities can be found in Table II for the two-tone cases, and in Table III for the three-tone cases.

L. Devaraj, Q. M. Khan, A. R. Ruddle, A. Duffy, R. Perdriau, and M. Koohestani, "Application of probabilistic models for multi-tone electromagnetic immunity analysis," IEEE Trans. Electromagn. Compat., 2022. doi: 110.1109/TEMC.2022.3211458.

From Tables I–III it can be seen that the failure probabilities for the multitone cases can be lower or higher than the single tone cases. Probabilistic models are needed to understand and analyse these phenomena.

Based on the simulation results, the probability of EMI failure was estimated for all of the two-tone and three-tone combinations. As noted above, the interactions between simultaneously occurring single-tones can either lead to positive causality or inhibition. For example, the individual probability of failures corresponding to single-tone disturbances having frequencies 50 MHz and 600 MHz are 0.849 and 0.904, respectively (see Table I), whereas when these two tones were superimposed fewer failures were observed (i.e., $\mathcal{P}(e|50, 600)$ = 0.779), corresponding to *inhibition*. Here, the inhibition may be due to the cancelling effect of the inter-modulation products of the two frequencies.

Probabilities corresponding to *no failure* and *complete failure* were replaced with 0.0001 and 0.9999 (respectively) for calculation purposes, and displayed in the tables as 0.0 and 1.0, respectively. This was done for two reasons; first, because finite data-sets cannot guarantee that failures are impossible or certain; and second, to avoid potential errors [14], [23] when applying probabilistic rules.

The leak probability (λ) for all noisy-OR multitone probability estimates is set to zero, as the steady-state response of the oscillator is always within the tolerable limits without EMI.

A. Synergistic Effects Due to Multitone EMI

Since reduced probability of failure is more desirable, inhibition is of less concern than positive causality. Multitone interactions with positive causality can be identified simply by checking whether the multitone failure probabilities exceed their corresponding single-tone values. The EMI failure probability for the two-tone combination $\mathbf{x} = \{450, 800\}$ (see Fig. 6) was found to be higher than those due to corresponding single-tones (see Figs. 2–3), indicating positive causality. This increased probability for harmonically related frequencies could be due to the individual or combined effect of the output frequency of the CSVCO being locked to one of the frequencies in the injected multitone disturbance and the inter-modulation products adding up. However, further investigation of the physical cause of the observed positive causality is beyond the scope of this paper. Furthermore, for each interaction identified to have positive causality, the difference $[\mathcal{P}(e|\,\mathbf{x}) - \mathcal{N}(e|\,\mathbf{x})]$ identifies synergy if it is > 0, or asynergy otherwise. Using the causal independence assumptions of noisy-OR (4), the probability for the case $\mathbf{x} = \{450, 800\}$, is:

$$\begin{aligned}\mathcal{N}(e|\,450, 800) &= 1 - \{(1 - \mathcal{P}(e|\,450))(1 - \mathcal{P}(e|\,800))\} \\ &= 1 - \{(1 - 0.653)(1 - 0.540)\} = 0.840 \end{aligned} \quad (7)$$

As $[\mathcal{P}(e|\,450, 800) - \mathcal{N}(e|\,450, 800)] > 0$, the interaction between these two tones is found to be synergistic.

The *degree of synergy* (*DoS*) is proposed as a useful metric for comparing relative changes in the probability of failure due

TABLE I
PROBABILITY OF EMI FAILURE DUE TO SINGLE-TONE DISTURBANCES OBTAINED FROM CASE STUDY A (CSVCO) SIMULATIONS

Single-tone (MHz)	50	100	200	300	350	450	500	550	600	650	700	750	800	900	950
$\mathcal{P}(e\|\,\mathbf{x})$	0.849	0.902	0.9	0.854	0.790	0.653	0.679	0.805	0.904	1.0	0.010	0.309	0.540	0.593	0.614

TABLE II
PROBABILITY OF EMI FAILURE DUE TO TWO-TONE DISTURBANCES OBTAINED FROM CASE STUDY A (CSVCO) SIMULATIONS

Two-tone (MHz)	50, 450,	50, 600,	50, 750,	50, 800,	50, 900,	450, 600,	450, 750,	450, 800,	450, 900,	600, 750,	600, 800,	600, 900,	750, 800,	750, 900,	800, 900,
$\mathcal{P}(e\|\,\mathbf{x})$	0.761	0.779	0.681	0.93	0.79	0.939	0.933	0.905	0.8	0.667	0.812	0.828	0.582	0.78	0.564
$\mathcal{N}(e\|\,\mathbf{x})$	0.948	0.986	0.896	0.931	0.939	0.967	0.761	0.840	0.859	0.934	0.956	0.961	0.682	0.719	0.813
DoS (%)	-19.8	-20.9	-24.1	-0.1	-15.8	-2.9	**22.7**	**7.7**	-6.9	-28.5	-15	-13.9	-14.7	**8.4**	-30.6
Causality	I	I	I	A	I	A	S	S	A	I	I	I	I	S	I

TABLE III
PROBABILITY OF EMI FAILURE DUE TO THREE-TONE DISTURBANCES OBTAINED FROM CASE STUDY A (CSVCO) SIMULATIONS

Three-tone (MHz)	50, 450, 600,	50, 450, 800,	50, 600, 750,	50, 600, 900,	50, 750, 900,	50, 800, 900,	450, 600, 750,	450, 600, 800,	450, 600, 900,	450, 750, 900,	450, 800, 900,	600, 750, 800,	600, 750, 900,	600, 800, 900,	750, 800, 900,
$\mathcal{P}(e\|\,\mathbf{x})$	0.691	0.522	0.996	0.809	1.000	0.667	0.744	0.846	0.863	1.000	0.798	0.572	0.785	0.630	0.622
$\mathcal{N}(e\|\,\mathbf{x})$	0.995	0.976	0.990	0.994	0.958	0.972	0.977	0.985	0.987	0.903	0.935	0.970	0.973	0.982	0.871
DoS (%)	-30.5	-46.5	**0.6**	-18.6	**4.4**	-31.4	-23.9	-14.1	-12.5	**10.8**	-14.7	-41.0	-19.3	-35.8	-28.6
Causality	I	I	S	I	S	I	I	I	I	S	A	I	I	I	A
$\mathcal{R}(e\|\,\mathbf{x})$	0.350	0.934	-1.360	-0.362	0.651	0.774	0.940	0.928	0.843	0.970	0.872	0.141	0.531	0.213	0.690
$\mathcal{R}_A(e\|\,\mathbf{x})$	0.991	0.986	0.990	0.994	0.967	0.972	0.988	0.983	0.965	0.970	0.945	0.960	0.979	0.982	0.867
$\mathcal{R}_I(e\|\,\mathbf{x})$	0.857	0.921	0.748	0.826	0.838	0.821	0.8949	0.934	0.920	0.970	0.849	0.821	0.841	0.787	0.779

L. Devaraj, Q. M. Khan, A. R. Ruddle, A. Duffy, R. Perdriau, and M. Koohestani, "Application of probabilistic models for multi-tone electromagnetic immunity analysis," IEEE Trans. Electromagn. Compat., 2022. doi: 110.1109/TEMC.2022.3211458.

to causal dependence between multitones. For any multitone, the *DoS* is calculated as a percentage using:

$$DoS = 100\left[\frac{\mathcal{P}(e|\,\mathbf{x}) - \mathcal{N}(e|\,\mathbf{x})}{\mathcal{N}(e|\,\mathbf{x})}\right] \tag{8}$$

A positive *DoS* strictly denotes synergy (highlighted and marked in Tables II, III, V and VI using *S*), whereas a negative *DoS* denotes either asynergy or inhibition (marked as *A* and *I*, respectively). For the two-tone example $\mathbf{x} = \{450, 800\}$ the *DoS* is 7.7%, thus indicating synergy. Other examples for asynergy and inhibition include the two-tone cases $\mathbf{x} = \{450, 600\}$ and $\mathbf{x} = \{50, 450\}$, respectively (see Table II).

B. Comparison of Two-Tone and Three-Tone Interactions

The interaction types of all 105 two-tone combinations considered for the analysis are summarized in Fig. 8. These results indicate 18 synergy, 24 asynergy and 63 inhibition type interactions. From a risk perspective, interactions between multitone disturbances that are identified as synergistic or asynergistic should be assessed further, especially if multitone disturbance is likely in the intended system environment. A similar analysis of the 455 three-tone cases (see Fig. 9) reveals 44 synergy, 103 asynergy and 308 inhibition interactions.

In this case-study, increasing the number of tones from two to three resulted in a decrease in the proportion of synergy and increase in the proportion of inhibition type interactions (see Fig. 10). Moreover, the average proportion of samples with synergy is higher for the two-tone EMI. The probability of failure due to three-tone EMI is lower due to the higher proportion of inhibition interactions.

V. Prediction of Multi-Causal Effects

A. Application of RNOR and ARNOR Rules

In order to validate the applicability of probabilistic theories discussed above, the RNOR rule is used to predict the probability of three-tone EMI failure using the probability values obtained from two-tone and single-tone simulations. For the three-tone combinations that are discussed in this section (see Table III), all the probability entries required to apply the rules of RNOR and other theories are provided (Tables I –II).

It can be seen from Fig. 8 that the interactions between some of the two-tone combinations are not of the positive causality type (i.e., synergy and asynergy), but are inhibition instead. As previously noted, the RNOR rule (5) is not applicable (indicated by negative values in Table III) if the calculation of three-tone failure probability involves any two-tone combinations that are of the inhibition type. For example, due to inhibition for the two-tone combination $\{50, 600\}$, the RNOR rule is not applicable for the combinations $\mathcal{R}(e|\,50, 600, 750)$ and $\mathcal{R}(e|\,50, 600, 900)$.

Whenever the RNOR rule may not be applicable, the ARNOR rule (6) was used to calculate the three-tone probability of failure. For example, the calculation of $\mathcal{R}(e|\,50, 600, 750)$, using (6) and the assumptions of ARNOR is:

$$\begin{aligned}\mathcal{R}_A(e|\,50, 600, 750) &= 1 - \left\{\left[\frac{1-\mathcal{N}(e|\,50, 600)}{1-\mathcal{P}(e|\,600)}\right]\right.\\ &\quad\left.\left[\frac{1-\mathcal{N}(e|\,600, 750)}{1-\mathcal{P}(e|\,750)}\right]\left[\frac{1-\mathcal{N}(e|\,750, 50)}{1-\mathcal{P}(e|\,50)}\right]\right\}\\ &= 1 - \left\{\left[\frac{1-0.986}{1-0.904}\right]\left[\frac{1-0.934}{1-0.309}\right]\left[\frac{1-0.896}{1-0.849}\right]\right\} = 0.990\end{aligned} \tag{9}$$

For the above example, without the use of ARNOR assumptions, the RNOR rule estimate would have provided $\mathcal{R}(e|\,50, 600, 750) = -1.3605$, which violates the Kolmogorov axioms of probability theory. It should be noted that when RNOR is applicable, $\mathcal{R}_A(e|\,\mathbf{x}) = \mathcal{R}(e|\,\mathbf{x})$ (e.g., case $\{450, 750, 900\}$).

B. Evaluation of Predictions: Noisy-OR vs ARNOR

To evaluate the predictive capability of ARNOR, the difference between the three-tone probabilities obtained from simulations, $\mathcal{P}(e|\,f_a, f_b, f_c)$, and ARNOR, $\mathcal{R}_A(e|\,f_a, f_b, f_c)$, were obtained for all of the three-tone combinations. The

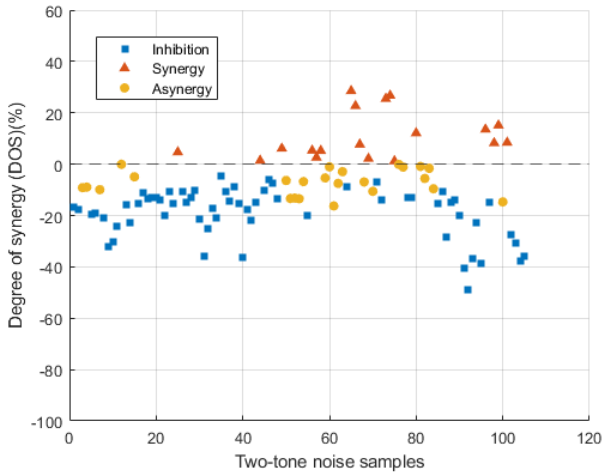

Fig. 8. Observed types of causal interaction in two-tone EMI simulations.

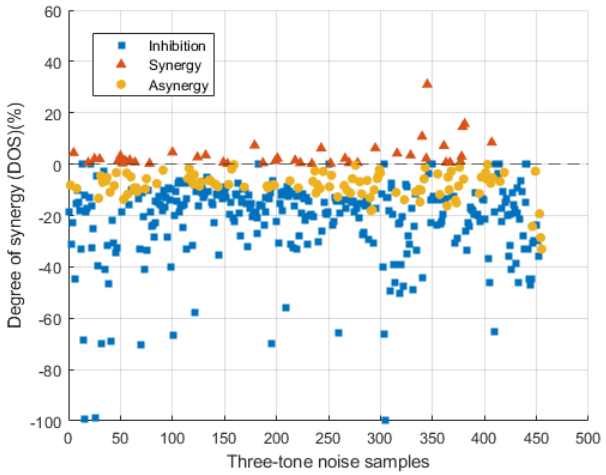

Fig. 9. Observed types of causal interaction in three-tone EMI simulations.

L. Devaraj, Q. M. Khan, A. R. Ruddle, A. Duffy, R. Perdriau, and M. Koohestani, "Application of probabilistic models for multi-tone electromagnetic immunity analysis," IEEE Trans. Electromagn. Compat., 2022. doi: 110.1109/TEMC.2022.3211458.

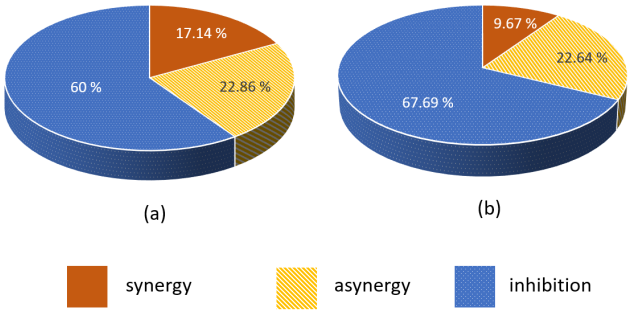

Fig. 10. Comparison between occurrence of causal interactions types for (a) two-tone, and (b) three-tone cases.

deviation of $\mathcal{R}_A(e|\,\mathbf{x})$ from $\mathcal{P}(e|\,\mathbf{x})$ is given in the histogram shown in Fig. 11. The mean deviation of the – 0.153, indicates that using the ARNOR rule might overestimate the probability values of three-tone EMI failure by 15%.

A similar comparison of mean deviation between $\mathcal{P}(e|\,f_a, f_b, f_c)$ and the noisy-OR, $\mathcal{N}(e|\,f_a, f_b, f_c)$ is shown in Fig. 12. In this case, the mean deviation was found to be – 0.159. The standard deviation ($\pm\sigma$) for both cases are similar at around ± 0.15. This shows that the RNOR and ARNOR predictions may not necessarily improve the predictive capability of empirical BN causal models to a large extent, when compared with the noisy-OR model that requires only the failure probabilities for individual causes.

C. Proposed Improvements to ARNOR Rule

To include available information on inhibitions observed between lower-order multi-causal interactions, some additional changes to the existing ARNOR rule are proposed. In the *improved ARNOR* (I-ARNOR) approach, the *DoS* corresponding to each probability entry is used as a correction factor to obtain revised probability estimates using:

$$\mathcal{R}_I(e|\,\mathbf{x}) = \mathcal{R}_A(e|\,\mathbf{x})\left[1 + \frac{0.01}{m}\sum_{i=1}^{m} DoS_m\right], \qquad (10)$$

where $m = r - 1$ and the factor 0.01 converts the *DoS* percentages back to fractions. In (10), DoS_m values corresponding to positive causality interactions are considered zero.

Using the I-ARNOR rule, the probability of EMI failure for the three-tone example $\{50, 600, 900\}$ is calculated as:

$$\begin{aligned}\mathcal{R}_I(e|\,50,600,900) = \\ \mathcal{R}_A(e|\,50,600,900)\left[1 + \frac{0.01}{3}(-20.9 - 13.9 - 15.8)\right] = \\ 0.994\left[1 + \frac{0.01}{3}(-50.6)\right] = 0.826 \qquad (11)\end{aligned}$$

For the above example, the probability of three-tone failure, estimated using I-ARNOR (0.826) is much closer to the failure probability estimated through simulations (0.809), when compared to the noisy-OR (0.994) and ARNOR (0.994) estimated values (also given in Table III). Other examples of the I-ARNOR rule applied for estimating the probability of three-tone EMI failures can be found in Table III. An effectiveness evaluation was also carried out for the I-ARNOR rule, as for the noisy-OR and ARNOR rules. As shown in Fig. 13, the mean deviation from simulated probability entries was estimated to be -0.0395, which is significantly smaller than the mean errors estimated for the existing noisy-OR and ARNOR rules. Although, the standard deviation estimated for the I-ARNOR predictions, $\sigma = 0.157$, is slightly greater than those obtained for the noisy-OR and ARNOR estimates, this represents a very small loss in precision compared to the marked improvement in terms of reduced bias in the mean value, delivering greater accuracy overall.

VI. Case Study B - Measured Data

Multitone immunity measurements on a ring oscillator (RO) circuit provide a second case study to both confirm the enhanced prediction capability of the proposed I-ARNOR model

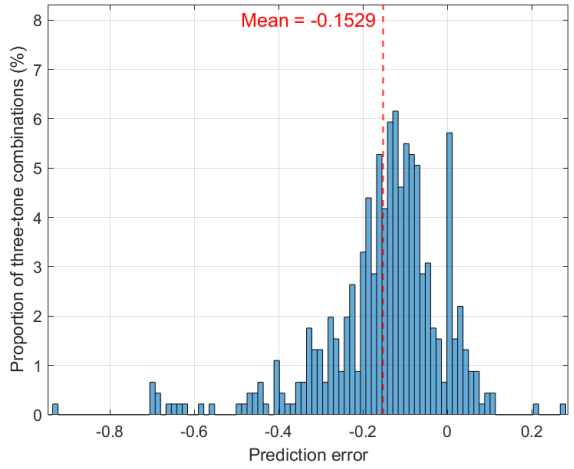

Fig. 11. Evaluation of ARNOR rule for prediction of multi-causal effect; μ_A = -0.15285 and σ_A = 0.15525.

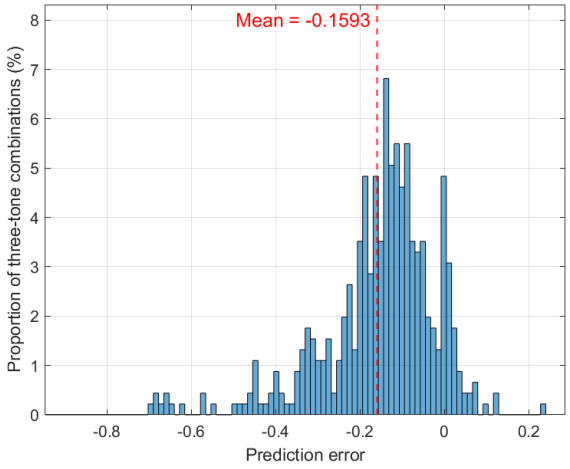

Fig. 12. Evaluation of noisy-OR rule for prediction of multi-causal effect; μ_N = -0.15929 and σ_N = 0.15283.

L. Devaraj, Q. M. Khan, A. R. Ruddle, A. Duffy, R. Perdriau, and M. Koohestani, "Application of probabilistic models for multi-tone electromagnetic immunity analysis," IEEE Trans. Electromagn. Compat., 2022. doi: 110.1109/TEMC.2022.3211458.

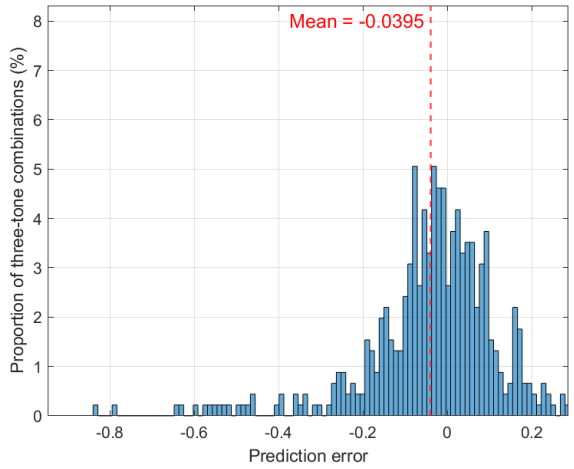

Fig. 13. Evaluation of I-ARNOR rule for prediction of multi-causal effect; μ_I = -0.039544 and σ_I = 0.15661.

and to demonstrate the wider applicability of this analysis method. A 13 cm x 13 cm 4-layer FR-4 printed circuit board (PCB) was designed using Altium for conducted immunity testing according to [1] with the IC in the center of the board. Furthermore, a 470 Ω resistor was included in series with the output pin of the RO circuit to limit high amplitude output voltage signals from being re-injected into the IC. A more detailed description of the IC and PCB design of the RO circuit are provided in [17].

A. Test Bench Setup

The experimental setup for the conducted multitone EMI immunity testing is shown in Fig. 14. Using a bias-tee (ZFBT-6GW+), the multitone EM disturbances generated from the vector signal generator (R&S SMM100A) were superimposed over the 5V power supply (KEYSIGHT E36313A). The output from the bias-tee was then injected into the input pin of the device under test (DUT) comprising the RO IC and associated ancillary circuits. The wider DUT circuits were powered by a separate 5V power supply that was entirely isolated from the EM disturbances. A signal and spectrum analyser (R&S FSVA3044) was used to observe the multitone disturbance generated by the vector signal generator. The DUT output signal was recorded using an oscilloscope (R&S RTM3004) for each injected multitone EM disturbance.

B. Test Plan and Limitations

The arbitrary function mode of the vector signal generator used to generate the multitone disturbance had a maximum clock frequency of 44 GHz and a fixed bandwidth of 600 MHz. The available combinations of two and three-tone disturbances were therefore limited by the 600 MHz bandwidth. To cover a broader range of frequencies for validation of the probabilistic models and to limit the total test time, two sets of frequencies were used, i.e., $\{100, 200, ..., 600\}$ MHz and $\{500, 600, ..., 1000\}$ MHz. Hence, a total of 10 single-tone, 29 two-tone and 40 three-tone disturbances were considered

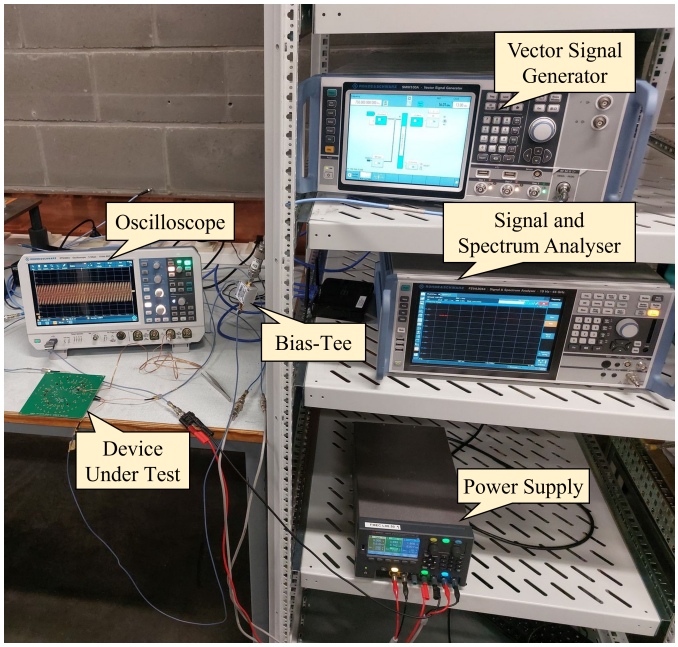

Fig. 14. Test bench setup for conducted multitone immunity testing

for Case Study B. Using the arbitrary waveform function, a constant power level of 10 dBm was assigned to each tone and the initial phase of each tone was randomly selected between −180° to 180°. The selected power was the minimum level at which the DUT showed an observable change in the output frequency without triggering the electrostatic discharge protection structures in the IC. As an example, the frequency spectrum of the three-tone combination $\{100, 400, 500\}$ MHz generated using the vector signal generator is shown in Fig. 15.

The resolution of the oscilloscope used to record the RO output signal was limited by a 2 GHz sampling rate, whereas 5 GHz sampling was used in the Cadence simulations for Case Study A. Moreover, a 3-stage frequency divider was used to monitor the output frequency of the RO (nominally F_2 = 955 MHz), which reduces the nominal output frequency to $F_2(AFD)$ = 97.7 MHz [17] and introduces additional uncertainties for the immunity measurements. The FFT of

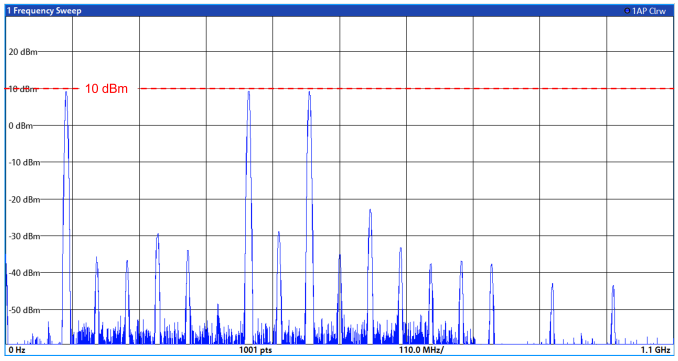

Fig. 15. Frequency spectrum of the three-tone combination $\{100, 400, 500\}$ MHz generated using the vector signal generator and measured with the signal and spectrum analyser. The power level of each tone is constant at 10 dBm.

L. Devaraj, Q. M. Khan, A. R. Ruddle, A. Duffy, R. Perdriau, and M. Koohestani, "Application of probabilistic models for multi-tone electromagnetic immunity analysis," IEEE Trans. Electromagn. Compat., 2022. doi: 110.1109/TEMC.2022.3211458.

the output signal over the entire time period for the three-tone disturbance $\{100, 400, 500\}$ MHz is illustrated in Fig. 16, showing the power levels of the injected frequencies to be lower than that of the RO output frequency. This is due to the effect of the IC output pad capacitance and package parasitics. The peak with the highest amplitude was considered as the output frequency of the DUT. For the case shown in Fig. 16 the shifted output frequency is F_E = 60 MHz and $\Delta F = -38.6\%$.

C. Multitone Immunity Performance Results

Considering the non-linear behaviour of the oscillator circuit, the FFT of the output signal is taken for every 35 ns over a steady-state time period of 3 µs for each measurement to determine the probability of failure using the failure criteria given in Section II.C. The total number of failures is then estimated using (1), where $F_i = F_2(AFD)$. See Fig. 17 for the RO output frequency observed during the injection of 3-tone disturbance $\{100, 400, 500\}$ MHz, where the probability of failure is 33.3%. The probability of EMI failure obtained from the measurements, $\mathcal{P}(e|\ \mathbf{x})$ for examples of single, two and three-tone disturbances are provided in Tables IV-VI. Comparison with the noisy-OR estimates again revealed

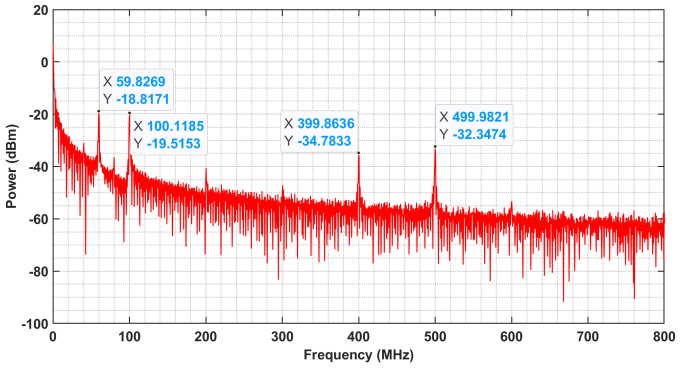

Fig. 16. Measured output frequency of the RO when injected with three-tone EM disturbance $\{100, 400, 500\}$ MHz.

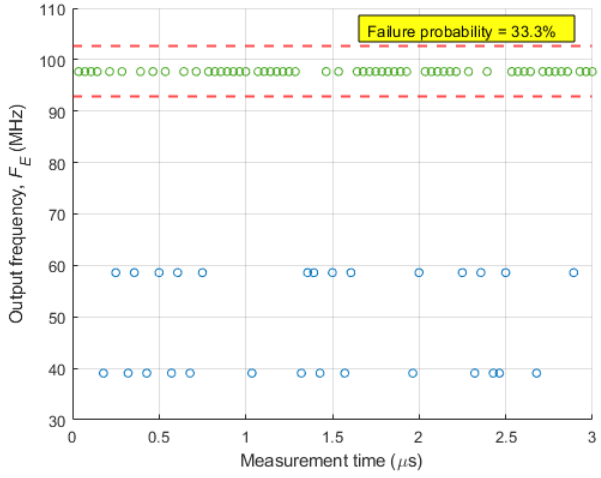

Fig. 17. RO output for three-tone disturbance at frequencies $\{100, 400, 500\}$ MHz.

synergy, asynergy and inhibition type interactions (see Tables V and VI). The magnitudes of the DoS for some measured higher-order multitone combinations were higher than seen in Case Study A: e.g., the DoS values for combinations $\{200, 400\}$ MHz, $\{400, 600\}$ MHz and $\{600, 800\}$ MHz are 230%, 639.5% and -99.9% (respectively). One specific reason for this behavior is that the RO is being locked to one of the injected multitone frequencies [17], creating a significant deviation from the nominal frequency. Additional measurement uncertainties may also contribute to this, but further investigation of these is beyond the scope of this paper.

D. Prediction Accuracy

The simulation results for Case Study A (CSVCO) were used to demonstrate the invalidity of the RNOR model and the improved mean prediction accuracy of the I-ARNOR model over the noisy-OR and ARNOR models. For experimental confirmation of this result, the three-tone failure probability values obtained for Case Study B (RO) are compared with the corresponding predictions made using the probabilistic models. The probability estimates using noisy-OR, RNOR, ARNOR and I-ARNOR models for some of the three-tone examples are given in Table VI. Histograms depicting the prediction errors for each model except RNOR (which is invalid) are shown in Figs. 18 to 20, confirming that the mean prediction error of the I-ARNOR model ($\mu_I = -0.0351$) is again much lower than the noisy-OR ($\mu_N = -0.1002$) and ARNOR ($\mu_A = -0.1855$) models. However, the standard deviation of the I-ARNOR model ($\sigma_I = 0.2086$) is higher than the noisy-OR model ($\sigma_N = 0.1760$), whereas lower than the ARNOR model ($\sigma_A = 0.2303$). The relative loss in precision of the I-ARNOR model with respect to the noisy-OR model in Case study B is due to the cancelling effect between three-tone disturbances, whose corresponding two-tone combinations have very high degree of synergy. For example, $\mathcal{P}(e|\ 400, 500, 600) = 0.25$, in-spite of one its two-tone combinations having $\mathcal{P}(e|\ 400, 600) = 0.875$ and $DoS = 629.5\%$. Except for such outliers, the three-tone predictions made by the I-ARNOR model remain superior to those of the existing noisy-OR derivatives.

VII. Conclusion

The application of various existing (noisy-OR, RNOR and ARNOR) and newly proposed (I-ARNOR) probabilistic models has been demonstrated in this paper for two different case studies, for the purposes of identifying the multi-causal interaction types between simultaneous EM disturbances and predicting the immunity performance of a component with respect to untested higher-order multitone disturbances. Based on the analysis of two different case studies, the noisy-OR model indicates the possibility of observing either increases or decreases in the probability of failure in comparison to single-tone disturbances. One of the reasons for the latter may be due to the inter-modulation products of the injected multitone disturbance adding up or cancelling out each other.

In real-world systems, positive causality of multitone disturbances means that unexpected component failures could be

L. Devaraj, Q. M. Khan, A. R. Ruddle, A. Duffy, R. Perdriau, and M. Koohestani, "Application of probabilistic models for multi-tone electromagnetic immunity analysis," IEEE Trans. Electromagn. Compat., 2022. doi: 110.1109/TEMC.2022.3211458.

TABLE IV
PROBABILITY OF EMI FAILURE DUE TO SINGLE-TONE DISTURBANCES OBTAINED FROM CASE STUDY B (RO) EXPERIMENTAL MEASUREMENTS

Single-tone (MHz)	100	200	300	400	500	600	700	800	900	1000
$\mathcal{P}(e\|\mathbf{x})$	0.33	0.011	0.606	0.063	0.017	0.059	0.042	0.031	0.092	0.095

TABLE V
PROBABILITY OF EMI FAILURE DUE TO TWO-TONE DISTURBANCES OBTAINED FROM CASE STUDY B (RO) EXPERIMENTAL MEASUREMENTS

Two-tone (MHz)	100, 400	100, 600	200, 400	200, 500	300, 400	300, 600	400, 500	400, 600	500, 600	500, 700	600, 800	600, 900	700, 900	700, 1000	800, 1000
$\mathcal{P}(e\|\mathbf{x})$	0.268	0.592	0.089	0.092	0.0	0.75	0.071	0.875	0.021	0.054	0.0	0.0	0.036	0.036	0.0
$\mathcal{N}(e\|\mathbf{x})$	0.372	0.369	0.074	0.028	0.631	0.629	0.079	0.118	0.074	0.058	0.088	0.145	0.13	0.133	0.123
DoS (%)	-28	**60.3**	**20.9**	**230.0**	-100.0	**19.3**	-9.67	**639.5**	-71.6	-7.5	-99.9	-99.9	-72.6	-73.1	-99.9
Causality	I	S	S	S	I	S	A	S	I	A	I	I	I	I	I

TABLE VI
PROBABILITY OF EMI FAILURE DUE TO THREE-TONE DISTURBANCES OBTAINED FROM CASE STUDY B (RO) EXPERIMENTAL MEASUREMENTS

Three-tone (MHz)	100, 200, 400	100, 200, 500	100, 300, 500	100, 400, 500	200, 300, 400	200, 400, 500	300, 400, 500	400, 500, 600	500, 600, 900	500, 700, 900	500, 800, 1000	600, 700, 900	600, 900, 1000	700, 900, 1000
$\mathcal{P}(e\|\mathbf{x})$	0.571	0.464	0.464	0.333	0.429	0.179	0.357	0.25	0.214	0.071	0.054	0.036	0.018	0.028
$\mathcal{N}(e\|\mathbf{x})$	0.739	0.376	0.751	0.383	0.633	0.085	0.635	0.103	0.087	0.135	0.126	0.172	0.157	0.204
DoS (%)	**50.7**	**33.3**	-37.3	-12.8	-32.5	**99.8**	-43.9	**87.8**	**34.1**	-50.7	-61	-80.3	-92.1	-86.8
Causality	S	S	I	A	S	S	I	S	S	I	I	I	I	I
$\mathcal{R}(e\|\mathbf{x})$	0.348	0.38	-0.658	0.194	-1.089	0.156	-1.34	0.869	-0.165	-0.067	-0.076	-0.136	-0.147	-0.048
$\mathcal{R}_A(e\|\mathbf{x})$	0.441	0.442	0.74	0.377	0.641	0.156	0.634	0.876	0.16	0.141	0.16	0.181	0.165	0.15
$\mathcal{R}_I(e\|\mathbf{x})$	0.4	0.411	0.348	0.315	0.27	0.156	0.24	0.667	0.015	0.06	0.053	0.039	0.055	0.077

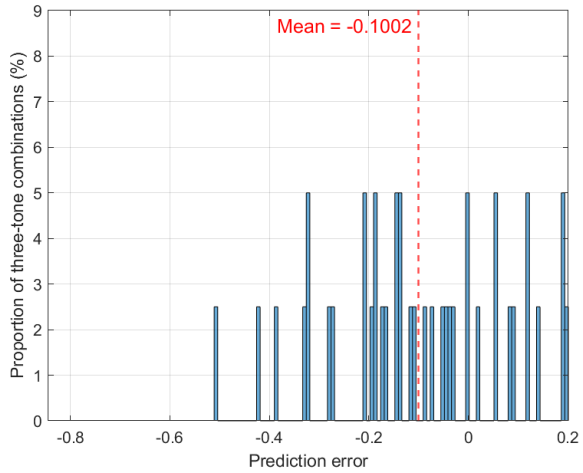

Fig. 18. Experimental evaluation of noisy-OR rule for prediction of multi-causal effect; μ_N = -0.1002 and σ_N = 0.1760.

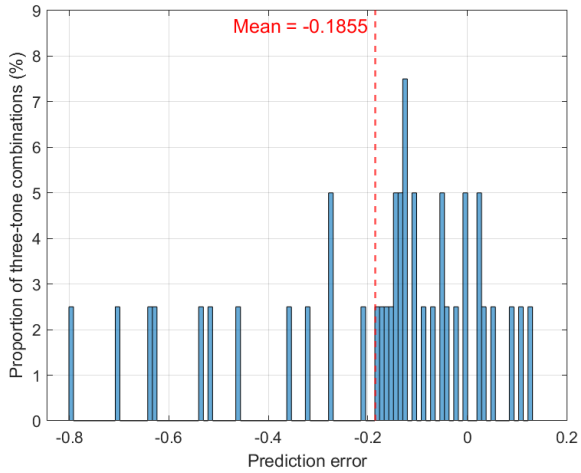

Fig. 19. Experimental evaluation of ARNOR rule for prediction of multi-causal effect; μ_A = -0.1855 and σ_A = 0.2303.

more likely in the systems' life-time than standard (single-tone) immunity tests might suggest. However, for multitone interactions that are identified as inhibition, the traditional single-tone immunity verification techniques can be considered a conservative approach.

To determine the maximum number of tones that need to be considered for multitone immunity investigations, the change in the proportion of synergy type interactions with increasing multitone order needs to be analysed. For acceptable proportions of synergy type interactions, the noisy-OR model can be used to estimate the multitone immunity performance, as those estimates will always be higher and provide a safety margin if the interactions are asynergy or inhibition.

A common limitation of multitone immunity analysis, for both simulations and measurements, is the exponential rise in the number of possible multitone combinations as the number of single-tones considered increases (note that conducted and radiated immunity measurements with more than 3 tones

L. Devaraj, Q. M. Khan, A. R. Ruddle, A. Duffy, R. Perdriau, and M. Koohestani, "Application of probabilistic models for multi-tone electromagnetic immunity analysis," IEEE Trans. Electromagn. Compat., 2022. doi: 110.1109/TEMC.2022.3211458.

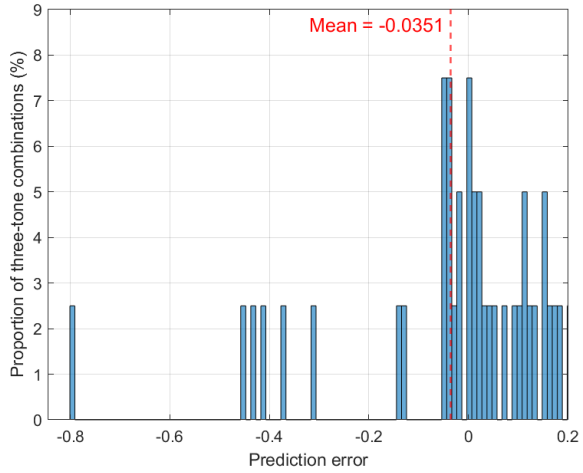

Fig. 20. Experimental evaluation of I-ARNOR rule for prediction of multi-causal effect; μ_I = -0.0351 and σ_I = 0.2086.

become impractical due to amplifier issues). However, the new I-ARNOR rule proposed herein can be applied in such cases to predict the failure probability of untested third or higher-order multitone combinations, at an accuracy much better than the existing models. Thus, these probabilistic methods could also complement and extend the current (or any future) immunity standard that includes multitone testing.

Using simulation data for a CSVCO circuit, the proposed I-ARNOR model was shown to have superior prediction accuracy to existing probabilistic models (i.e., the noisy-OR and ARNOR models). The simulations offered advantages such as higher sampling rate and bandwidth as well as freedom to monitor signals at inaccessible traces. Measurements, however, are subject to practical limitations such as PCB trace parasitics, cable losses, and other uncertainties that are not included in the simulations. For these reasons, as well as to demonstrate wider applicability, experimental validation of the I-ARNOR probabilistic model was provided for a different (RO) circuit.

Furthermore, the influence of temperature on the multitone immunity performance of oscillator circuits has also been experimentally investigated and successfully analysed [17] using the probabilistic models discussed in this paper. Further investigation of the applicability of the extended-RNOR model to predict the probability of higher order ($r > 3$) multitone EMI failures could be undertaken using the available data (for $r \leq 3$). For example, from (2) an additional 1,365 simulations corresponding, to all possible four-tone ($r = 4$) combinations of $n = 15$ frequencies, would be required to obtain the validation data.

Acknowledgement

This publication reflects only the authors' view, exempting the European Union from any liability. Project website: http://etn-peter.eu/. The authors would like to thank Dr. Tim Claeys from KU Leuven campus Bruges (Belgium) for providing access to multitone immunity test facilities.

References

[1] IEC 62132-4: 2006, *Integrated circuits — Measurement of electromagnetic immunity 150 kHz to 1 GHz — Part 4: Direct RF power injection method*, 2006.

[2] M. Mardiguian, "Combined effects of several, simultaneous, EMI couplings," in *Proc. IEEE Int. Symp. on Electromagn. Compat. Symp. Record (Cat. No.00CH37016)*, vol. 1, 2000, pp. 181–184 vol.1.

[3] A. Biondi, H. Rogier, D. Vande Ginste, and D. De Zutter, "Multi-tone EMC testing strategy for RF-devices," in *Proc. 2012 IEEE Elect. Des. of Adv. Packag. and Syst. Symp. (EDAPS)*, 2012, pp. 89–92.

[4] G. Barth, "Benefits of multitone EMC immunity testing," *Int. Jrnl. RF Microw. Comput.-Aided Eng.*, vol. 26, pp. 355–358, May 2016.

[5] A. Duffy, A. Orlandi, and K. Armstrong, "Preliminary study of a reverberation chamber method for multiple-source testing using intermodulation," *IET Sci., Meas. Technol.*, vol. 4, pp. 21 – 27, 02 2010.

[6] A. Biondi, F. Declercq, D. D. Zutter, H. Rogier, and L. Vallozzi, "Electromagnetic compatibility aware design and testing of intermodulation distortion under multiple co-located sources illumination," *IET Sci. Meas. Technol.*, vol. 6, pp. 105–112, 2012.

[7] IEC 61000-4-3:2020-09 (EN), *Electromagnetic compatibility (EMC) - Testing and measurement techniques. Radiated, radio-frequency, electromagnetic field immunity test*, 2020.

[8] K. Armstrong, "Testing for immunity to simultaneous disturbances and similar issues for risk managing EMC," in *Proc. 2012 IEEE Int. Symp. on Electromagn. Compat.*, 2012, pp. 121–126.

[9] A. Ephrath, D. Weiner, and G. Capraro, "Statistical analysis of digital circuits subjected to EMI induced delays," in *Proc. 1984 National Symp. on Electromagn. Compat.*, 1984, pp. 1–1.

[10] A. Ephreth, D. Weiner, G. Capraro, and C. Paludi, "A probabilistic approach to EMC modeling and analysis," in *Proc. 1982 IEEE Int. Symp. on Electromagn. Compat.*, 1982, pp. 1–4.

[11] E. Genender, H. Garbe, and F. Sabath, "Probabilistic risk analysis technique of intentional electromagnetic interference at system level," *IEEE Trans. Electromagn. Compat.*, vol. 56, no. 1, pp. 200–207, 2014.

[12] C. Mao and F. Canavero, "System-level vulnerability assessment for EME: From fault tree analysis to Bayesian networks—Part I: Methodology framework," *IEEE Trans. Electromagn. Compat.*, vol. 58, no. 1, pp. 180–187, 2016.

[13] J. Pearl, "Chapter 4 - Belief updating by network propagation," in *Probabilistic Reasoning in Intelligent Systems*. San Francisco (CA): Morgan Kaufmann, 1988, pp. 143–237. [Online]. Available: https://www.sciencedirect.com/science/article/pii/B9780080514895500102

[14] J. Lemmer and D. Gossink, "Recursive noisy OR - a rule for estimating complex probabilistic interactions," *IEEE Trans. Syst., Man, and Cybern., Part B (Cybern.)*, vol. 34, no. 6, pp. 2252–2261, 2004.

[15] V. Anand and S. M. Downs, "An empirical validation of recursive noisy OR (RNOR) rule for asthma prediction," in *Proc. AMIA Annu. Symp.*, Nov. 2010, p. 16—20.

[16] D. A. Quintanar-Gago and P. F. Nelson, "The extended recursive noisy OR model: static and dynamic considerations," *Int. J. Approx. Reasoning*, vol. 139, pp. 185–200, 2021. [Online]. Available: https://www.sciencedirect.com/science/article/pii/S0888613X21001559

[17] Q. M. Khan, L. Devaraj, R. Perdriau, A. R. Ruddle, T. Claeys, M. Ramdani, and M. Koohestani, "Experimental characterization of multitone em immunity of integrated oscillators under thermal stress," *IEEE Access*, vol. 10, pp. 83 898–83 915, 2022.

[18] B. Razavi, "Chapter 14 - Oscillators," in *Design of Analog CMOS Integrated Circuits*. New York, NY 10121: McGraw-Hill Education, 2001.

[19] Q. M. Khan, L. Devaraj, M. Koohestani, A. R. Ruddle, M. Ramdani, and R. Perdriau, "Synergistic effect of multitone EMI on the conducted immunity of integrated oscillators," *IEEE Letters on Electromagnetic Compatibility Practice and Applications*, vol. 4, no. 3, pp. 77–82, 2022.

[20] Q. M. Khan, A. Ramezani, M. Koohestani, M. Ramdani, and R. Perdriau, "A comparison among DPI immunities of multi-stage CSVCOs and ring oscillators," in *Proc. 2021 13th Int. Workshop on the Electromagn. Compat. of Integr. Circuits (EMC Compo)*, 2022, pp. 123–127.

[21] "Cadence Virtuoso (2021). Spectre Simulation Platform," https://www.cadence.com/ko_KR/home/tools/custom-ic-analog-rf-design/circuit-simulation/spectre-simulation-platform.html, [Online; accessed 2022-02-08].

[22] A. Boyer and É. Sicard, *Basis of Electromagnetic Compatibility of Integrated Circuits: A Modelling Approach Using IC-EMC*, ser. Pour l'ingénieur. Presses Universitaires du Midi, 2017. [Online]. Available: https://books.google.co.uk/books?id=LewxswEACAAJ

L. Devaraj, Q. M. Khan, A. R. Ruddle, A. Duffy, R. Perdriau, and M. Koohestani, “Application of probabilistic models for multi-tone electromagnetic immunity analysis,” IEEE Trans. Electromagn. Compat., 2022. doi: 110.1109/TEMC.2022.3211458.

[23] D. Koller and N. Friedman, *Probabilistic Graphical Models: Principles and Techniques - Adaptive Computation and Machine Learning*. MIT Press, 2009.
[24] M. Henrion, “Practical issues in constructing a Bayes’ Belief Network,” in *Proc. Third Conf. on Uncertainty in Artif. Intell. (UAI’87)*, 1987, p. 132–139.
[25] Y. Xiang and N. Jia, “Modeling causal reinforcement and undermining for efficient CPT elicitation,” *IEEE Trans. Knowledge Data Eng.*, vol. 19, no. 12, pp. 1708–1718, 2007.
[26] S. P. Woudenberg, L. C. van der Gaag, and C. M. Rademaker, “An intercausal cancellation model for Bayesian-Network engineering,” *Int. J. Approx. Reasoning*, vol. 63, no. C, p. 32–47, aug 2015. [Online]. Available: https://doi.org/10.1016/j.ijar.2015.05.011
[27] F. J. Díez and M. J. Druzdzel, “Canonical probabilistic models for knowledge engineering,” UNED, Madrid, Spain, Tech. Rep., CISIAD-06-01, 2006.

Lokesh Devaraj (Student Member, IEEE) received the B.E. degree in electronics and communication engineering from Anna University, Chennai, India, in 2017 and received the M.Sc. degree in advanced optical technologies from the Freidrich Alexander University, Erlangen, Germany, in 2019. Currently, he is working toward the Ph.D. degree in electrical and electronic engineering from the De Montfort University, Leicester, U.K. As a part of the MSCA ETN PETER, he will carry out research on the Risk – Based Automotive Electromagnetic Engineering Approach aligned with the ISO 26262 Functional Safety Approach. Since 2019 he is also working as an automotive electronic research engineer in the vehicle resilience department of HORIBA MIRA Limited, Nuneaton, U.K. His research interests include risk-based EMC, functional safety, cybersecurity and statistical models.

Qazi Mashaal Khan (Graduate Student Member, IEEE) received the Bachelor’s degree in Electrical Engineering from FAST NUCES university, Pakistan, in 2016, with summa cum laude. He finished the Joint Master’s Degree in Smart Systems Integration with distinction in 2019. This was an EU funded Erasmus + Program where he spent his four semesters in UK, Norway, Hungary and Germany. The host was Heriot-Watt University, UK. He is currently working towards his Ph.D. research at the Radio and Hyper-frequency (RF) and the Electromagnetic Compatibility (EMC) group at ESEO, France. As part of the MSCA ETN PETER, he will carry out the extension of the IC Immunity and Emission models to incorporate environmental stresses. His Doctoral Degree will be provided by INSA Rennes University. His research interests include ageing, thermal stresses and obsolescence on EMC behavior on many categories of ICs.

Alastair R. Ruddle (M’09–SM’17) received the B.Sc. degree in physics in 1983 from the University of Bristol, Bristol, U.K. and the Ph.D. degree in electronic and electrical engineering from the University of Loughborough, Loughborough, U.K.

Since 1996 he has been with HORIBA MIRA Limited, Nuneaton, U.K., an automotive research and technology organization. He is currently Chief Scientist for Vehicle Resilience Technologies. His research interests include computational electromagnetics, electromagnetic measurements, human exposure to electromagnetic fields and cybersecurity. He is the author/coauthor of more than 160 publications, including articles published in journals and presented at international symposia as well as book chapters. Dr. Ruddle is registered as a Chartered Physicist and a Chartered Engineer in the UK, and participates in a number of international standards activities relating to human exposure to electromagnetic fields and CEM validation. Prior to joining HORIBA MIRA he carried out research in a number of disciplines in the defense and power industries.

Alistair P. Duffy (SM’04, F’14), is Professor of Electromagnetics and Director of the Institute of Engineering Sciences at De Montfort University (DMU), Leicester, UK. He received his BEng (Hons) and MEng degrees in 1988 and 1989, respectively, from University College, Cardiff, University of Wales. He read for his PhD with professors Christopoulos and Benson at Nottingham University, graduating in 1993. He also holds an MBA from the Open University, UK, graduating in 2004. He was awarded his DSc from Cardiff University in 2019 for his body of research on the validation of computational electromagnetics. He is a Fellow of the IEEE and past President of the IEEE EMC Society. He has published approximately 300 papers, mostly on his research interests of validation of computational electromagnetics; physical layer components, particularly communications cabling, and electromagnetic compatibility testing.

Richard Perdriau (M’01-SM’07) was born in Angers, France, in 1971. He received the engineering degree in electronics and computer science from ESEO Angers - Grande Ecole d’Ingénieurs Généralistes, Angers, France, in 1992, the Ph.D. degree in applied sciences from Université Catholique de Louvain, Louvain-la-Neuve, Belgium, in 2004, and the “Habilitation à Diriger des Recherches” (Accreditation Degree) from Université de Rennes 1, Rennes, France, in 2012.

From 1992 to 2012, he was an Associate Professor with ESEO School of Engineering in the fields of microelectronics and embedded systems. In 2013, he became a Full Professor. His research interests include EMC of integrated circuits, mixed-signal hardware description languages, and integrated circuit design. Dr. Perdriau served as the Vice-Chair and the Technical Program Co-Chair of EMC Europe 2017. In January 2020, he was elected as the Secretary of the IEEE France Section.

Mohsen Koohestani (Senior Member, IEEE) received the PhD degree (Hons.) in electromagnetics from the école polytechnique fédérale de Lausanne (EPFL), Lausanne, Switzerland, and the Universidade de Lisboa (ULISBOA), Lisbon, Portugal, in 2014.

From 2014 to 2018, he was a senior research fellow with the Institut d’Electronique et de Télécommunications de Rennes (IETR), University of Rennes 1, working mainly on biomedical applications of wireless power transfer systems. He is presently an Associate professor at ESEO School of Engineering, Angers, France (since 2018). He is also an associate researcher at IETR, UMR CNRS 6164. He has authored over 60 peer-reviewed scientific papers. His main interests lie in the domain of antennas, microwaves, EMC, and biomedical engineering.

Dr. Koohestani is an official member of the IEC standardization working group (WG2 & WG9) in the SC47A French subcommittee on the EMC for integrated circuits.